

Photonic synthesis of high fidelity microwave arbitrary waveforms using near field frequency to time mapping

Amir Dezfooliyan^{1,*} and Andrew M. Weiner^{1,2}

¹ School of Electrical and Computer Engineering, Purdue University, 465 Northwestern Avenue, West Lafayette, Indiana 47907-2035, USA

² Birck Nanotechnology Center, Purdue University, 1205 West State Street, West Lafayette, Indiana 47907, USA
*amir@purdue.edu

Abstract: Photonic radio-frequency (RF) arbitrary waveform generation (AWG) based on spectral shaping and frequency-to-time mapping has received substantial attention. This technique, however, is critically constrained by the far-field condition which imposes strict limits on the complexity of the generated waveforms. The time bandwidth product (TBWP) decreases as the inverse of the RF bandwidth which limits one from exploiting the full TBWP available from modern pulse shapers. Here we introduce a new RF-AWG technique which we call near-field frequency-to-time mapping. This approach overcomes the previous restrictions by predistorting the amplitude and phase of the spectrally shaped optical signal to achieve high fidelity waveforms with radically increased TBWP in the near field region.

©2013 Optical Society of America

OCIS codes: (060.5625) Radio frequency photonics; (320.5540) Pulse shaping; (350.4010) Microwaves.

References and links

1. M. Z. Win and R. A. Scholtz, "Ultra-wide bandwidth time-hopping spread-spectrum impulse radio for wireless multiple-access communications," *IEEE Trans. Commun.* **48**(4), 679–689 (2000).
2. M.-G. Benedetto, T. Kaiser, A. F. Molisch, I. Oppermann, C. Politano, and D. Porcino, *UWB communication systems A comprehensive overview* (Hindawi Publishing Corporation, 2006).
3. A. Dezfooliyan and A. M. Weiner, "Evaluation of time domain propagation measurements of UWB systems using spread spectrum channel sounding," *IEEE Trans. Antenn. Propag.* **60**(10), 4855–4865 (2012).
4. J. D. McKinney, D. E. Leaird, and A. M. Weiner, "Millimeter-wave arbitrary waveform generation with a direct space-to-time pulse shaper," *Opt. Lett.* **27**(15), 1345–1347 (2002).
5. J. Chou, Y. Han, and B. Jalali, "Adaptive RF-photonics arbitrary waveform generator," *IEEE Photon. Technol. Lett.* **15**(4), 581–583 (2003).
6. I. S. Lin, J. D. McKinney, and A. M. Weiner, "Photonic synthesis of broadband microwave arbitrary waveforms applicable to ultra-wideband communication," *IEEE Microw. Wirel. Compon. Lett.* **15**(4), 226–228 (2005).
7. V. Torres-Company, J. Lancis, and P. Andres, "Arbitrary waveform generator based on all-incoherent pulse shaping," *IEEE Photon. Technol. Lett.* **18**(24), 2626–2628 (2006).
8. J. Capmany and D. Novak, "Microwave photonics combines two worlds," *Nat. Photonics* **1**(6), 319–330 (2007).
9. C. Wang and J. Yao, "Photonic generation of chirped millimeter-wave pulses based on nonlinear frequency-to-time mapping in a nonlinearly chirped fiber bragg grating," *IEEE Trans. Microw. Theory Tech.* **56**(2), 542–553 (2008).
10. M. H. Khan, H. Shen, Y. Xuan, L. Zhao, S. Xiao, D. E. Leaird, A. M. Weiner, and M. Qi, "Ultrabroad-bandwidth arbitrary radiofrequency waveform generation with a silicon photonic chip-based spectral shaper," *Nat. Photonics* **4**(2), 117–122 (2010).
11. J. Yao, "Photonics for ultrawideband communications," *IEEE Microw. Mag.* **10**(4), 82–95 (2009).
12. A. M. Weiner, "Femtosecond pulse shaping using spatial light modulators," *Rev. Sci. Instrum.* **71**(5), 1929–1960 (2000).
13. J. Azana and M. A. Muriel, "Real-time optical spectrum analysis based on the time-space duality in chirped fiber gratings," *IEEE J. Quantum Electron.* **36**(5), 517–526 (2000).
14. V. Torres-Company, D. E. Leaird, and A. M. Weiner, "Dispersion requirements in coherent frequency-to-time mapping," *Opt. Express* **19**(24), 24718–24729 (2011).

15. A. Dezfouliyan and A. M. Weiner, "Temporal focusing of ultrabroadband wireless signals using photonic radio frequency arbitrary waveform generation," *Optical Fiber Commun. Conf. (OFC)*, pp. 1–3 (Anaheim, Calif., 2013).
16. S. Shen and A. M. Weiner, "Complete dispersion compensation for 400-fs pulse transmission over 10-km fiber link using dispersion compensating fiber and spectral phase equalizer," *IEEE Photon. Technol. Lett.* **11**(7), 827–829 (1999).
17. A. M. Weiner, *Ultrafast Optics* (Wiley, 2009).
18. C. Wang and J. Yao, "Chirped microwave pulse generation based on optical spectral shaping and wavelength-to-time mapping using a sagnac loop mirror incorporating a chirped fiber bragg grating," *J. Lightwave Technol.* **27**(16), 3336–3341 (2009).
19. B. H. Kolner, "Space-time duality and the theory of temporal imaging," *IEEE J. Quantum Electron.* **30**(8), 1951–1963 (1994).
20. M. T. Kauffman, A. A. Godil, B. A. Auld, W. C. Banyai, and D. M. Bloom, "Applications of time lens optical systems," *Electron. Lett.* **29**(3), 268–269 (1993).
21. A. M. Weiner, D. E. Leaird, J. S. Patel, and J. R. Wullert, "Programmable shaping of femtosecond optical pulses by use of 128-element liquid-crystal phase modulator," *IEEE J. Quantum Electron.* **28**(4), 908–920 (1992).
22. J. T. Willits, A. M. Weiner, and S. T. Cundiff, "Line-by-line pulse shaping with spectral resolution below 890 MHz," *Opt. Express* **20**(3), 3110–3117 (2012).
23. S. Xiao and A. M. Weiner, "Coherent photonic processing of microwave signals using spatial light modulators: programmable amplitude filters," *J. Lightwave Technol.* **24**(7), 2523–2529 (2006).
24. A. J. Metcalf, V. Torres-Company, V. R. Supradeepa, D. E. Leaird, and A. M. Weiner, "Fully programmable ultra-complex 2-D pulse shaping," *Conf. of Lasers and Electro-Optics (CLEO)*, pp. 1–2 (San Jose, Calif., 2012).

1. Introduction

Ultrabroadband arbitrary radio-frequency (RF) waveforms with large time bandwidth product (TBWP) are relevant to a variety of applications including radar imaging and high-data rate covert wireless communications [1–3]. Due to limits associated with digital-to-analog convertors, electronic AWGs have a restricted RF bandwidth. Although recently offering increased bandwidth approaching 18 GHz, electronic solutions suffer large timing jitter and may be difficult to deploy in harsh environments characterized for example by high electromagnetic interference (EMI). On the other hand, photonic approaches [4–10] are generally immune to EMI, provide ultrabroad bandwidth and support remoting applications [11].

Photonic techniques for RF-AWG based on spectral shaping and frequency-to-time mapping (FTM) [5–10] have enjoyed special attention. In this technique, the desired RF waveform is programmed onto the optical power spectrum using a pulse shaping element [12]. The shaped pulses are then stretched in a dispersive medium where the chromatic dispersion provides the so called frequency-to-time mapping phenomenon [5–10, 13, 14]. This method, however, is subject to the so-called *far-field* condition, which imposes a minimum amount of dispersion and limits the complexity of signals that can be handled. For RF-AWG, this condition imposes an onerous limit on the amount of information that can be placed on to the signal, severely restricting the TBWP. The TBWP decreases as the inverse of the RF bandwidth and becomes disappointingly small for RF bandwidth beyond those already available with electronic arbitrary waveform generators.

In this paper, we propose a new technique to circumvent this limitation to frequency-to-time mapping. We predistort the amplitude and phase of the spectrally shaped optical signal to achieve high fidelity waveforms at the near field region, enabling generation of waveforms not accessible under the far-field condition. In this technique, which we call Near-Field Frequency-to-Time Mapping (NF-FTM), the maximum achievable TBWP can be maintained over a wide RF bandwidth range which is quite distinct from the conventional FTM approach. The unique generated waveforms with unprecedented instantaneous RF bandwidth offer potential for new horizons in areas such as chirped radar, high-speed covert wireless, and RF sensing [15].

For most of this paper, we assume linear frequency-to-time mapping, i.e., frequency-to-time mapping in a medium with linear group velocity dispersion. In principle, the spectral shaping of the input signal can be modified to account for or compensate a limited amount of

higher order dispersion terms such as dispersion slope, e.g [16]. However, this point is not pursued here.

The remainder of this paper is organized as follows. Section 2 mathematically describes the conventional FTM approach and the limitations imposed by the far-field criterion. In section 3, we explain the near-field frequency-to-time mapping approach and derive the limitations and the achievable TBWP for this technique. Section 4 presents a numerical simulation to show unique advantages of the new proposed technique. Section 5 describes our experimental setup and provides an example in which we generate an ultrabroadband RF quadratic chirp signal over the frequency range of nearly baseband up to 41 GHz with the time aperture of 6.8 ns. We show while this signal can be generated easily by the NF-FTM technique with high fidelity, the conventional FTM technique results in a very badly distorted signal. The waveform generated under NF-FTM is in close agreement with simulation. Finally, Section 6 discusses the main implications of the work, and in Section 7 we summarize.

2. Frequency-to-time mapping

Here we cover the basics of the conventional linear frequency-to-time mapping method and derive the relation between the maximum RF bandwidth and time aperture under the far-field condition. To facilitate discussion, we show frequency and time domain variables for optical and RF signals in Fig. 1. For optical waveforms, which are of a passband nature, the bandwidth (B) is defined as the difference between the highest and lowest (nonzero)

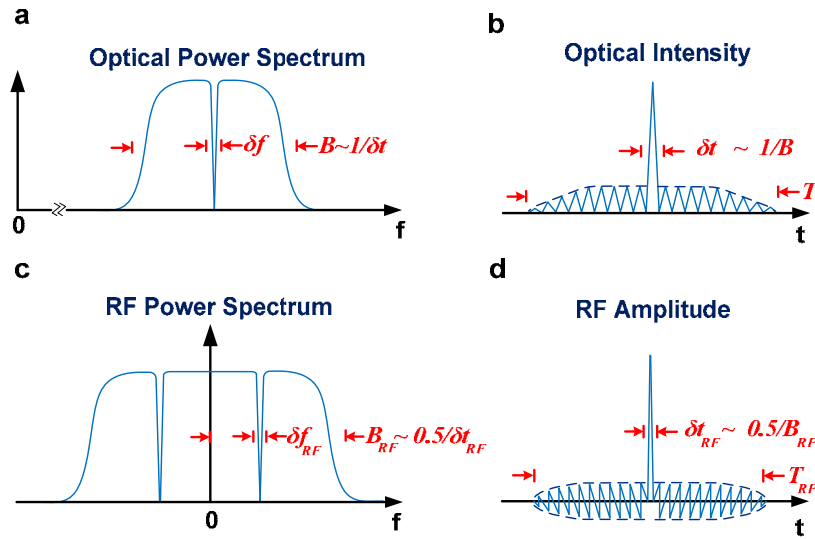


Fig. 1. (a-b) Frequency and time domain variables for optical waveforms. (c-d) Frequency and time domain variables for RF waveforms. We use subscript “RF” for all RF quantities.

Table 1. Variables and their meaning.*

Symbol	Meaning	Symbol	Meaning
δt	Optical temporal resolution	δt_{RF}	RF temporal resolution
T	Optical time aperture	T_{RF}	RF time aperture
B	Optical bandwidth	B_{RF}	RF bandwidth
δf	Optical spectral resolution	Δf_{inst}	Instantaneous frequency shift – optical
$\delta \phi$	Applied phase change at a given time sample	$TBWP$	Time bandwidth product

*Optical variables refer to the shaped signal prior to dispersive propagation.

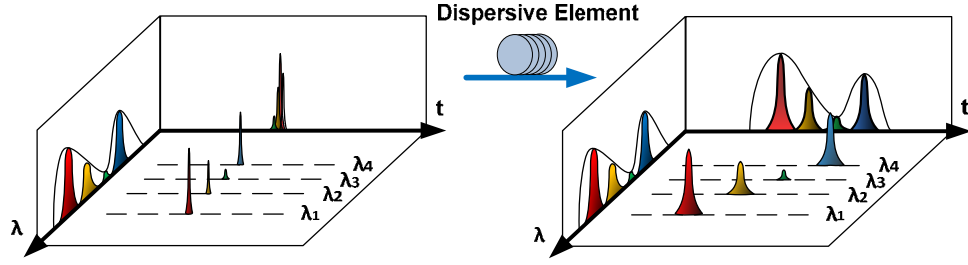


Fig. 2. Frequency-to-time mapping phenomenon. When the shaped spectrum propagates through a dispersive element, different wavelengths travel at different speeds (only four wavelengths are shown for illustration). For sufficiently large chromatic dispersion, we get a linear frequency-dependent time delay which maps the power spectrum to the temporal intensity profile.

frequency components, Fig. 1(a). Here we assume that the spectral phase variation in the optical signal is sufficiently slow so that the duration of the temporal waveform is determined by the amplitude spectral variations in the input pulse, not by the phase variations. As a result, the shortest temporal feature, δt , is inversely related to the total bandwidth by $\delta t \sim 1/B$, and the maximum temporal window, T , is inversely related to the optical spectral resolution, δf , by $T \sim 1/\delta f$. By contrast, for the baseband RF waveforms, the RF bandwidth, B_{RF} , is defined as the highest frequency component, as shown in Fig. 1(c). B_{RF} is inversely related to twice the RF temporal resolution, δt_{RF} , by $B_{RF} \sim 0.5/\delta t_{RF}$, consistent with the logic that two time samples are required to represent an RF cycle. These variables are all summarized in Table 1.

Figure 2 shows the linear frequency-to-time mapping phenomenon. The desired waveform is programmed onto the optical power spectrum using a pulse shaping element (e.g. Fourier transform pulse shaper [12]). When the shaped spectrum propagates through a dispersive element with chromatic dispersion, different wavelengths travel at different speeds. For large enough dispersion, we get a linear frequency-dependent time delay which maps the power spectrum to the temporal intensity profile.

Mathematically, the transformation of a pulse propagating in a medium with group delay dispersion (ψ_2) can be expressed by the Fresnel integral [17]:

$$a_{out}(t) \propto \exp\left(-j \frac{t^2}{2\psi_2}\right) \int_{-\infty}^{+\infty} a_{in}(t') \exp\left(-j \frac{t'^2}{2\psi_2}\right) \exp\left(j \frac{t t'}{\psi_2}\right) dt'. \quad (1)$$

where $a_{in}(t)$ and $a_{out}(t)$ are respectively the complex envelopes of the signals before and after the dispersive medium. Here ψ_2 is the group delay dispersion which is defined as $\psi_2 = -\partial^2 \beta(\omega)/\partial \omega^2 L$ where $\beta(\omega)$ is the propagation constant of the medium with length L . In some applications, notably fiber optics the fiber dispersion is usually described in terms of a dispersion parameter D with units $ps \, nm^{-1} \, km^{-1}$, related to the group delay dispersion as $\psi_2 = (\lambda^2 D)/(2\pi c)L$ where λ is the wavelength and c is the speed of light.

To facilitate our later discussion, we introduce the notation $a_{FTM}(t)$ to denote the shaped input field $a_{in}(t)$ associated with the frequency-to-time mapping. When the so called *far-field* limit is satisfied, the temporal phase variation associated with the $\exp(-jt^2/2\psi_2)$ factor within the integral is negligible [13, 14, 17]. To be definite, in the analysis that follows we require that the phase variation within a time duration equal to the inverse of the finest spectral feature placed onto the input spectrum should be $< \pi/8$. Although this requirement is closely related to the far-field condition, it is more accurately termed the “antenna designer’s formula” in [14]. To keep the language simple, in this paper we will refer simply to the “far-

field condition". Under this condition, the output intensity profile is simply a scaled replica of the optical power spectrum, i.e.,

$$|a_{out}(t)|^2 \stackrel{\substack{\text{Far Field} \\ \text{Limit}}}{\propto} \left| \exp\left(-j \frac{t^2}{2\psi_2}\right) \int_{-\infty}^{+\infty} a_{FTM}(t') \exp\left(j \frac{t t'}{\psi_2}\right) dt' \right|^2 = |A_{FTM}(\omega = -t/\psi_2)|^2. \quad (2)$$

where $A_{FTM}(\omega)$ is the Fourier transform of $a_{FTM}(t)$. Here, we take the definition of the Fourier transform of a function $f(t)$ as $F(\omega) = \int f(t') \exp(-j\omega t') dt'$. Equation (2) shows that the detected intensity profile after frequency-to-time mapping is proportional to the Fourier transform of the input signal at the angular frequency $\omega = -t/\psi_2$. For RF-AWG, the input power spectrum is shaped as $|A_{FTM}(\omega = -t/\psi_2)|^2$, which is taken to be equal to the desired RF waveform $|a_{out}(t)|^2$, appropriately scaled. Although Eq. (2) indicates that when the far-field limit is satisfied, the spectral phase of $A_{FTM}(\omega = -t/\psi_2)$ can be arbitrary chosen [7], we use a flat spectral phase for experiments and simulations in this paper.

A critical bottleneck in this method, however, is the minimum required dispersion (ψ_{2-min}) to meet the far-field criterion. As explained above, this condition corresponds to tolerating phase errors up to $\pi/8$ within the quadratic factor $\exp(-jt^2/2\psi_2)$ of the Fresnel integral [13, 14]:

$$\left| \frac{(T/2)^2}{2\psi_2} \right| < \frac{\pi}{8} \Rightarrow \frac{T^2}{\pi} < |\psi_2| \Rightarrow |\psi_{2-min}| = \frac{T^2}{\pi} \approx \frac{1}{\pi \delta f^2}. \quad (3)$$

This requirement directly imposes strict limits on the complexity and bandwidth of the achievable RF waveforms if arbitrary electrical waveforms are to be generated with high fidelity (low distortion):

$$B_{RF} \approx \frac{0.5}{\delta t_{RF}} \stackrel{2\pi \delta f = \delta t_{RF} |\psi_2|}{=} \frac{0.5}{2\pi \delta f |\psi_2|} < \frac{0.5}{2\pi \delta f |\psi_{2-min}|} \stackrel{(3)}{\approx} 0.25 \times \delta f. \quad (4)$$

Here we have assumed that the minimum duration RF features (δt_{RF}) are determined by frequency-to-time mapping of the finest optical spectral features (δf). Equation (4) shows that the maximum achievable RF bandwidth of the conventional FTM method is proportional to the optical spectral resolution. To synthesize an undistorted RF waveform with larger frequency content, a coarser spectral resolution is required which limits one from exploiting the full TBWP of modern pulse shapers.

Working at the maximum RF bandwidth permitted under Eq. (4), the RF time aperture (T_{RF}) can be expressed as:

$$T_{RF} \approx N \delta t_{RF} = \frac{B}{\delta f} \delta t_{RF} \approx B \frac{1}{\delta f} \frac{0.5}{B_{RF}} \stackrel{(4)}{\approx} B \frac{0.25}{B_{RF}} \frac{0.5}{B_{RF}} \approx \frac{0.125}{(B_{RF})^2} B. \quad (5)$$

where $N = T/\delta t = B/\delta f$ is the ratio of the time aperture and temporal resolution of the shaped optical signal prior to dispersive propagation, or equivalently the ratio of the optical bandwidth and finest spectral feature. In this regime, the TBWP is:

$$TBWP_{FTM} \stackrel{(5)}{\approx} \frac{0.125B}{B_{RF}}. \quad (6)$$

Equation (6) shows the $TBWP_{FTM}$ is inversely proportional to the required RF bandwidth and becomes disappointingly small for RF bandwidth beyond those already available with electronic arbitrary waveform generators. Although experiments reaching bandwidths beyond the limit presented in Eq. (6) have been reported [18], the failure of these experiments to satisfy the far-field condition and the consequent significant loss of fidelity to generate arbitrary RF waveforms have apparently gone unnoticed.

3. Near-field frequency-to-time mapping

Here, we introduce a new technique which uses the amplitude and phase programmability of the shaper to overcome limitations imposed by the far-field requirement and achieve arbitrary nondistorted waveforms with the maximum available TBWP. In this approach, which we call Near-Field Frequency-to-Time Mapping (NF-FTM), the pulse shaper is programmed to yield a complex envelope $a_{NF-FTM}(t)$ represented by:

$$a_{NF-FTM}(t) = a_{FTM}(t) \exp\left(j \frac{t^2}{2\psi_2}\right). \quad (7)$$

where as mentioned above, $a_{FTM}(t)$ is defined in terms of the target RF waveform assuming frequency-to-time mapping strictly applies. Here $a_{FTM}(t)$ is multiplied by a new quadratic phase term that cancels out the phase factor $\exp(-jt^2/2\psi_2)$ in Eq. (1). As a result the target waveform $|a_{out}(t)|^2$ that appears in the frequency-to-time mapping expression, Eq. (2), is obtained exactly independent of the far-field condition. Experimentally we realize this condition simply by reprogramming the pulse shaper according to the Fourier transform of Eq. (7); no new physical device is needed.

From another viewpoint, Eq. (7) is reminiscent of time lens [19, 20] studies in which physical elements such as electro-optic phase modulators or nonlinear wave mixing generate quadratic temporal phase. However, in our scheme we compute the effect of the quadratic temporal phase to arrive at a complex optical spectrum, which we then program in the optical frequency domain. Since there is no physical element providing direct time domain phase, we can consider our new approach as assisted by a virtual-time-lens. The waveform predistortion prescribed under this method advances the location at which the Fourier transform relation of Eq. (2) applies from the far-field into the near-field region, enabling generation of waveforms not accessible under the far-field condition.

3.1 Theory of near-field frequency-to-time mapping

As mentioned for the FTM technique, a phase error of $\pi/8$ is tolerable in the Fresnel integral. Hence, the quadratic phase introduced in Eq. (7) does not necessarily need to exactly cancel out the phase factor $\exp(-jt^2/2\psi_2)$ in Eq. (1) to produce the desired RF waveforms. This makes our new NF-FTM method tolerant of small phase errors that may arise in experimental systems.

3.1.1 Maximum RF bandwidth limit

Here, we analyze the ability to realize the operation specified by Eq. (7) using a Fourier transform pulse shaper. The assumed temporal quadratic phase implies time-varying frequency shifts away from the initial frequency content. Since pulse shaping is taken as a time invariant operation, which does not increase optical bandwidth, a main requirement for physical realizability is that the spectral broadening that would accompany the quadratic temporal phase remains small compared to the optical bandwidth. Here, we follow this logic to establish a limit on the maximum temporal quadratic phase that may be introduced.

The phase shift of the n th temporal feature (ϕ_n) of the quadratic factor applied in Eq. (7) can be written as:

$$\phi_n = \frac{\delta t^2 (n - N/2)^2}{2\psi_2} \quad 1 \leq n \leq N. \quad (8)$$

Where N , as defined above, is the total number of resolvable features of the pulse shaper. The maximum phase change from one temporal feature to the next ($\delta\phi_{max}$) which occurs at the edges of the quadratic phase is:

$$\delta\phi_{\max} = |\phi_N - \phi_{N-1}| \stackrel{(8)}{=} \frac{\delta t^2}{2|\psi_2|} (N-1) \approx \frac{\delta t^2}{2|\psi_2|} N = \frac{\delta t^2}{2|\psi_2|} \frac{B}{\delta f} \stackrel{\delta t \sim 1/B}{\approx} \frac{1}{B} \frac{1}{2|\psi_2| \delta f}. \quad (9)$$

Using the fact that the detected intensity profile is proportional to the Fourier transform of the input signal at the angular frequency $\omega = -t/\psi_2$, we have:

$$\delta\phi_{\max} \stackrel{(9)}{\approx} \frac{1}{B} \frac{1}{2|\psi_2| \delta f} \stackrel{2\pi \delta f = \delta t_{RF}/|\psi_2|}{=} \frac{\pi}{B} \frac{1}{\delta t_{RF}} \stackrel{\delta t_{RF} \sim 0.5/B_{RF}}{\approx} \frac{2\pi}{B} B_{RF}. \quad (10)$$

Equation (10) shows the maximum applied temporal phase shift ($\delta\phi_{\max}$) is proportional to the ratio of the generated RF bandwidth (B_{RF}) to the optical bandwidth. Although the applied temporal quadratic phase shift is essential to get a faithful frequency to time mapping in the near field region, it remains small except at very high RF bandwidth such that B_{RF} approaches the optical bandwidth. For example for ultrabroadband waveforms with bandwidth in the range of ~ 10 to ~ 100 GHz, the B_{RF} is orders of magnitude smaller than the optical bandwidth (optical bandwidth of 5 THz is assumed), and the corresponding $\delta\phi_{\max}$ is limited to the range of only $\sim 0.004\pi$ to $\sim 0.04\pi$.

To estimate the maximum spectral broadening that would be introduced by a true quadratic temporal phase factor, we use the principle of the instantaneous frequency shift (Δf_{inst}) [17]. This parameter is defined in terms of the time derivative of the applied temporal phase ($\delta\phi$) as:

$$\Delta f_{\text{inst}} = \frac{1}{2\pi} \frac{\delta\phi}{\delta t} \leq \frac{1}{2\pi} \frac{\delta\phi_{\max}}{\delta t} \stackrel{\delta t \sim 1/B}{\approx} \frac{\delta\phi_{\max}}{2\pi} B \stackrel{(10)}{\approx} B_{RF}. \quad (11)$$

Equation (11) shows the instantaneous frequency shift that would accompany a true quadratic temporal phase is proportional to the target RF bandwidth. This equation reconfirms our conclusion derived based on Eq. (10) from another viewpoint. The spectral broadening that would accompany the quadratic phase factor remains considerably small unless the RF bandwidth approaches the optical bandwidth. For example, when we seek to generate an RF signal with maximum bandwidth in the range of 10 to 100 GHz, the corresponding spectral broadening implied by the quadratic phase factor is limited to the range of only 0.2% to 2% of the initial optical spectrum bandwidth (optical bandwidth of 5 THz is assumed).

The Δf_{inst} calculated in Eq. (11) is the shift we would get if we multiplied by a real quadratic phase. Since we cannot increase the optical bandwidth in our method (since we employ time invariant spectral shaping, which implements a virtual not a real time lens), we require the implied instantaneous frequency shift (or equivalently the RF bandwidth) to be much smaller than optical spectrum bandwidth. Otherwise the near-field frequency-to-time mapping process will be disturbed.

$$\Delta f_{\text{inst}} \stackrel{(11)}{\approx} B_{RF} \ll B \quad \Leftrightarrow \quad \delta\phi_{\max} \ll 2\pi. \quad (12)$$

As a conservative bound, we limit the instantaneous frequency shift (or equivalently the RF bandwidth) to be smaller than one-eighth of the optical bandwidth (B) (e.g., for a pulse shaper with 5 THz spectral bandwidth, this number is roughly 625 GHz). This means that NF-FTM can be applied over a very wide microwave frequency range while maintaining waveform fidelity, which is quite distinct from conventional FTM. From another viewpoint, this condition is equivalent to limiting the maximum temporal phase change from one feature to the next to be smaller than $\pi/4$:

$$\delta\phi_{\max} \stackrel{(10)}{\approx} \frac{2\pi}{B} B_{RF} \xrightarrow{B_{RF} < 0.125 \times B} \delta\phi_{\max} < \frac{\pi}{4}. \quad (13)$$

This condition is in close agreement with the results of a series of numerical simulations we have performed considering bandwidth, pixelation and resolution limitations of the pulse shapers. Some simulation examples are provided in section 4 and 5.3.

3.1.2 Time aperture versus RF bandwidth

For the generated microwave waveforms within the limit of Eq. (12), in which the implied instantaneous frequency shift remains much smaller than the optical spectral bandwidth, the time aperture and the maximum RF bandwidth are related as:

$$T_{RF} = N \delta t_{RF} = \frac{B}{\delta f} \delta t_{RF} \stackrel{\delta t_{RF} \sim 0.5/B_{RF}}{\approx} \frac{B}{\delta f} \frac{0.5}{B_{RF}}. \quad (14)$$

In this regime, the achievable time bandwidth product (TBWP) can be estimated by:

$$TBWP_{NF-FTM} \approx 0.5 \frac{B}{\delta f}. \quad (15)$$

As we see from Eq. (15), the $TBWP_{NF-FTM}$ in near-field frequency-to-time mapping is only a function of pulse shaper's characteristics. In particular, the available TBWP is equal to one half the number of spectrally resolved control elements within the optical bandwidth. As long as Eq. (12) is satisfied, $TBWP_{NF-FTM}$ is directly proportional to the optical bandwidth and is independent of the targeted RF bandwidth. This is in contrast to Eq. (6), for which the $TBWP_{FTM}$ in conventional frequency-to-time mapping was inversely proportional to the required RF bandwidth.

4. Simulation results

Here we simulate generation of a linear down-chirp signal (instantaneous frequency changes linearly with time) with time aperture of ~ 125 ns and RF bandwidth of ~ 20 GHz, corresponding to a TBWP of 2500. The pulse shaper is simulated based on the model presented in [17, 21] which includes the finite bandwidth of the input field, the finite spectral resolution of the pulse shaper associated with the finite spot size of any single frequency component at the Fourier plane, and the pixellated nature of the spatial light modulator employed in the pulse shaper. In this simulation, a pulse shaper with 25125 pixels, optical spectral resolution of 1 GHz, and total optical bandwidth of 5.025 THz (corresponds to the lightwave C band) is used. Although such a pulse shaping experiment is beyond any reported yet, pulse shapers with resolution well below 1 GHz have already been demonstrated [22, 23], as have programmable shapers with thousands of individually controllable elements at a few GHz spectral resolution configured in a novel two-dimensional spectral dispersion geometry [24]. Thus, this example is chosen to motivate the potential to generate high fidelity RF arbitrary waveforms through NF-FTM even for pulse shapers that challenge the state-of-the-art.

The output of the pulse shaper is stretched through a dispersive medium with total group delay dispersion of 3.125 ns/nm to yield a time aperture of 125 ns (higher order dispersion is not included in this simulation). Figure 3(a) shows the target waveform programmed onto the power spectrum, assuming frequency-to-time mapping applies. The roll-off (loss of modulation contrast) for the short wavelength portion of Fig. 3(a) arises because the desired spectral modulation is approaching the pulse shaper spectral resolution. As explained in [17, 21], the effect of pulse shaper resolution can be modeled by convolving with a Gaussian signal in the frequency domain, which introduces attenuation for spectral modulation that is too rapid.

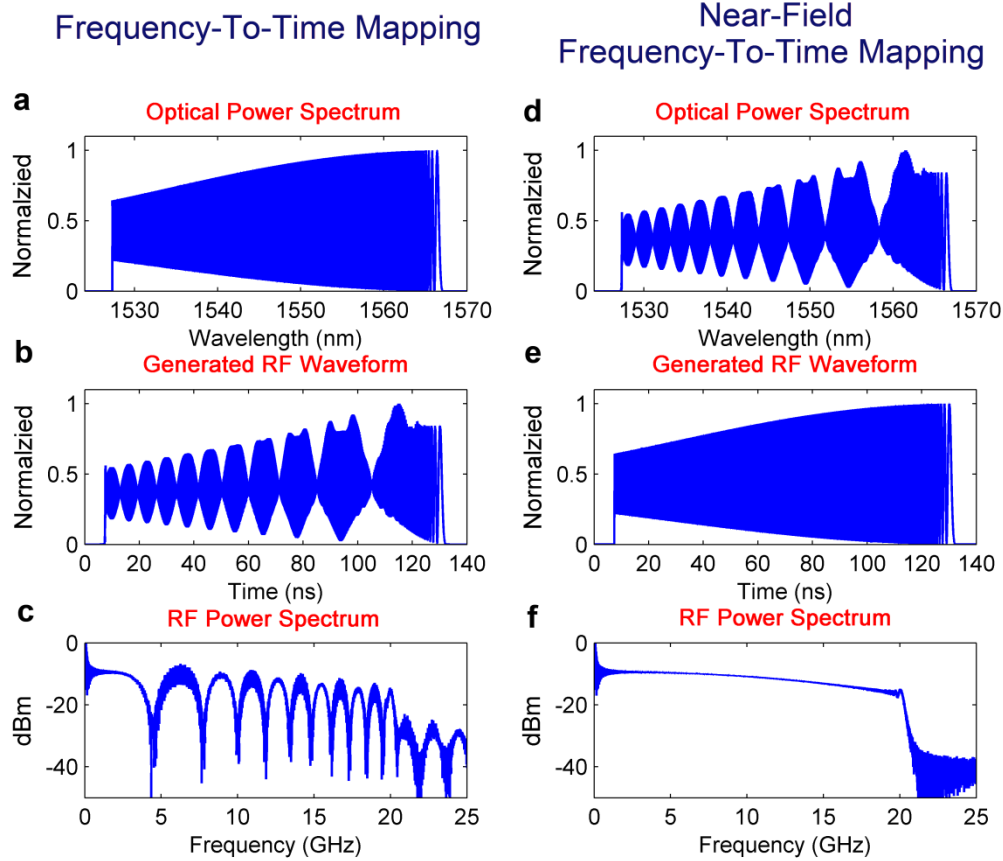


Fig. 3. Simulating the generation of a linear down-chirp RF waveform over frequencies from baseband to ~ 20 GHz with time aperture of ~ 125 ns, corresponding to a TBWP of ~ 2500 . (a-c) Waveforms from conventional frequency-to-time mapping. The generated RF waveform is badly distorted, and certain frequencies are strongly attenuated. (d-f) Waveforms from near-field frequency-to-time mapping. An undistorted chirp is obtained, and the RF spectrum extends smoothly out to ~ 20 GHz.

In this example in which we use a total dispersion of 3.125 ns/nm, the far-field limit is strongly violated. Equation (3) shows for pulse shaping with a finest spectral feature of 1 GHz, the far-field limit is satisfied only for dispersions larger than ~ 250 ns/nm. Here, the maximum temporal phase variation (in the quadratic phase term inside the integral of Eq. (1)) is $\sim 10\pi$ within a time duration equal to the inverse of finest spectral feature placed onto the spectrum by the pulse shaper. This is much larger than the maximum allowed value ($\pi/8$) in the far-field criterion. As a result the generated RF waveform, Fig. 3(b), is badly distorted, and certain groups of frequencies are strongly attenuated, Fig. 3(c).

Now, we use near-field frequency-to-time mapping to circumvent the far-field condition. To avoid any possible confusion, we would like to emphasize that the required temporal quadratic phase required to advance the Fourier plane into the near-field region is several orders of magnitude smaller than the spectral phase induced by the dispersive medium (e.g. optical fibers). For instance in this example, the total unwrapped spectral phase arising due to passage through the dispersive medium is $\sim 1.6 \times 10^5 \pi$, while the maximum temporal phase required to implement the virtual time lens is only $\sim 10\pi$.

Figure 3(d) shows the optical power spectrum shaped according to Eq. (7) based on NF-FTM. In this example in which a flat spectral phase is assumed for $a_{FTM}(t)$, the optical power

spectrum for NF-FTM, Fig. 3(d), is a scaled replica of the temporal distortion of Fig. 3(b). A simple derivation explaining this scaling relationship is presented as an appendix. Although Fig. 3(d) shows only the power spectrum, the corresponding field must have the spectral phase function as prescribed by NF-FTM. This is unlike FTM, where input spectral phase does not affect output power spectrum. When this pre-distorted signal propagates through the dispersive medium, a time domain RF waveform with undistorted chirp is obtained, Fig. 3(e), which is indistinguishable from the target waveform—refer to Fig. 3(a), appropriately scaled. The RF spectrum of this signal, Fig. 3(f), extends smoothly out to ~ 20 GHz with less than 6.5 dB roll-off in respect to the 1 GHz frequency component.

5. Experiment

5.1 Experimental setup

The experimental setup is shown in Fig. 4. An erbium-doped fiber ring mode-locked laser with repetition rate of ~ 50 MHz and wavelength range of ~ 1520 nm–1610 nm is used as the input source. The laser pulses are shaped with a commercial pulse shaper (FINISAR 1000s)

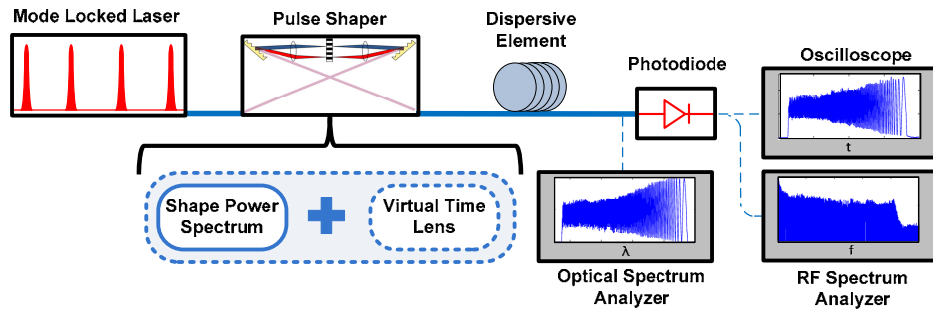


Fig. 4. Experimental setup (only main components are shown). Output pulses of a mode-locked laser are sent through a pulse shaper with spectral resolution of ~ 10 GHz. The pulse shaper can be programmed either according to the conventional FTM method in which the desired waveform is sculpted onto the optical power spectrum or according to the Near-Field Frequency-to-Time mapping (NF-FTM) algorithm. In NF-FTM the spectral shaping of FTM is modulated as prescribed by an assumed quadratic temporal phase factor (virtual time lens) resulting in both amplitude and phase spectral shaping. In either case, the generated signals are stretched in a dispersive element, and then the RF signals are detected by a high-speed photodiode (PD).

with spectral resolution of ~ 10 GHz and operating wavelength range of 1527.4 nm–1567.4 nm. The output pulses are stretched in ~ 10.3 km of single mode fiber with total dispersion of ~ 170 ps/nm and dispersion slope of ~ 0.57 ps/nm². In the experiments we program the pulse shaper assuming only linear group delay dispersion. Higher order dispersion is taken into account in the simulations to most closely model the experiment. The RF signal is detected by a high-speed photodetector with bandwidth of ~ 50 GHz. A digital sampling oscilloscope and an RF spectrum analyzer with respective bandwidths of 60 GHz and 50 GHz are used to characterize the generated RF waveforms in time and frequency. The optical spectrum is also measured with an optical spectrum analyzer with spectral resolution of 0.01 nm.

5.2 Experimental result

We illustrate the limits of conventional FTM with an experiment in which we seek to generate a quadratic down-chirp waveform with ~ 41 GHz bandwidth and ~ 6.8 ns time aperture. The instantaneous frequency is designed to decrease monotonically from 41 GHz down to baseband according to a concave-down quadratic function of time. Assuming frequency-to-time mapping applies, the target waveform is written onto the power spectrum, Fig. 5(a). However, for this example, for which the variation of the temporal quadratic phase

term within the integral of Eq. (1) reaches $\sim 1.84\pi$, the far-field criterion is strongly violated. As a result the generated RF waveform, Fig. 5(b), is badly distorted, and certain groups of frequencies are strongly attenuated, Fig. 5(c). To comply with the far-field condition, Eq. (4) dictates that in order to synthesize an RF waveform with spectrum up to 41 GHz, the pulse

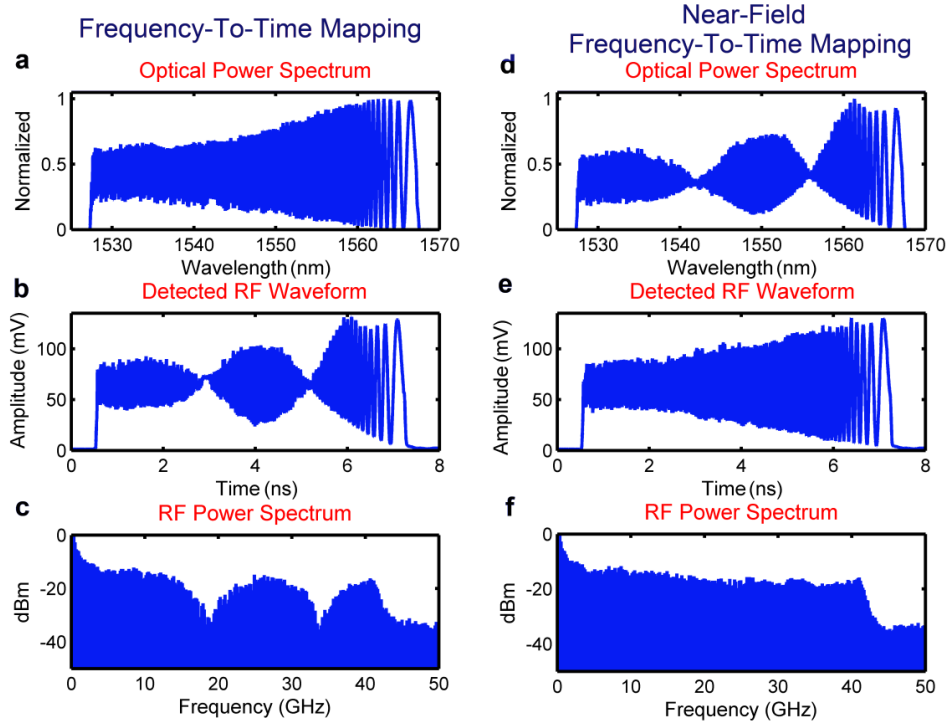


Fig. 5. Generating down-chirp RF waveform over frequencies from baseband to ~ 41 GHz with time aperture of ~ 6.8 ns, corresponding to a TBWP of ~ 280 . (a-c) Waveforms from conventional frequency-to-time mapping. Generated RF waveform is badly distorted and certain frequencies are strongly attenuated. (d-f) Waveforms from near-field frequency-to-time mapping. An undistorted chirp signal is obtained and the RF spectrum extends smoothly out to ~ 41 GHz with less than 5 dB roll-off in respect to the 4 GHz frequency components.

shaper should be programmed with super-pixels with minimum resolution of ~ 164 GHz (Eq. (4)), much coarser than the ~ 10 GHz spectral resolution capability of the pulse shaper. This would reduce the maximum possible TBWP of the synthesized waveform to < 17 (Eq. (6)) for frequency-to-time mapping free of significant distortion.

To overcome the limitations of the far-field condition, we use the proposed NF-FTM. Figure 5(d) shows the new optical power spectrum which now shows strong predistortions that closely resemble the temporal distortions of Fig. 5(b). Unlike previously, the shaped field is necessarily programmed with spectral phase variation as well; however, this is not visible in a plot of the power spectrum. After dispersive propagation a time domain RF waveform with undistorted chirp is obtained, Fig. 5(e), in close agreement with the target waveform – refer to Fig. 5(a), appropriately scaled. Here due to the pulse shaper spectral resolution, the high frequency modulations of the chirp signal shows an amplitude roll-off compared to later, low frequency components.

Removing constraints imposed by the far-field criterion, a TBWP of ~ 280 , near the maximum possible using this pulse shaper, is now achieved. The RF spectrum, Fig. 5(f), extends smoothly out to ~ 41 GHz with less than 5 dB roll-off with respect to the 4 GHz frequency components. This is more than a factor of two beyond the highest bandwidth available from commercial electronic arbitrary waveform generators. This combination of

high RF bandwidth and large TBWP, while maintaining excellent waveform fidelity, is unprecedented in photonic RF-AWG.

5.3 Verification of the experiment

To evaluate the experimental accuracy of the synthesized waveforms via our proposed NF-FTM method, we compare the generated chirp waveform shown in Fig. 5(e) with a numerical

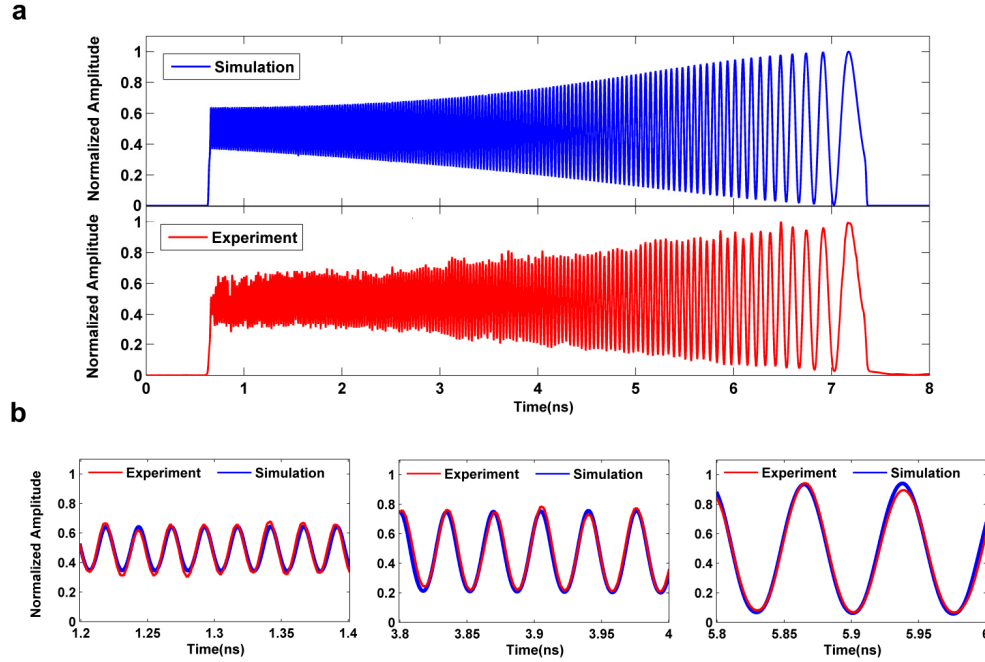


Fig. 6. (a) Experimental result versus simulation for the generated chirp waveform with time aperture of ~ 6.8 ns and bandwidth of ~ 41 GHz. (b) we overlay these curves on top of each other and zoom in on different parts of the waveform to show details. The agreement between the simulation and experimental results is excellent.

simulation result. For the simulations in this section, a pulse shaper with 5025 pixels, optical spectral resolution of 10 GHz, and total optical bandwidth of 5.025 THz (corresponds to the lightwave C band) is modeled, which is the same as the parameters of the commercial pulse shaper (Finisar WaveShaper 1000s) used in our experiments. The output waveform from the pulse shaper is stretched through a dispersive medium with total group delay dispersion of ~ 170 ps/nm and dispersion slope of ~ 0.57 ps/nm² to yield a time aperture of ~ 6.8 ns (here the dispersion slope is included to allow meaningful comparison of experimental and simulation results). The effect of the dispersion slope with our experimental parameters is to increase the frequency span of the generated chirp function by $<4\%$ compared to the targeted frequency span.

Figure 6 compares the experimental result with simulation. The agreement between the two curves is excellent. In Fig. 6(b), we overlay these curves on top of each other and zoom in on different parts of the waveform to show details. We can see the simulation and the experiment match peak for peak and there are at most a few percent differences between them. The correlation coefficient between these two curves is on the order of 99.2%, which shows an extremely good match between simulation and experimental results.

6. Discussion

In Fig. 7, we show upper bound estimations of the RF bandwidth and time aperture achievable from the conventional FTM and NF-FTM techniques for two shapers with assumed spectral resolutions of 1 GHz and 10 GHz. In both cases we have assumed 5 THz optical bandwidth, corresponding to the lightwave C band. Conventional FTM is restricted to the space below the far-field limit (Eq. (5)) for which good waveform fidelity is maintained, whereas NF-FTM is bounded only by the optical bandwidth (Eq. (12) and (13)) and pulse shaper resolution (Eq. (14)) limits. In NF-FTM the maximum achievable TBWP, which is directly proportional to the number of pulse shaping pixels resolved within the optical bandwidth, can be maintained over a wide RF bandwidth range. However, in conventional FTM a coarser spectral resolution

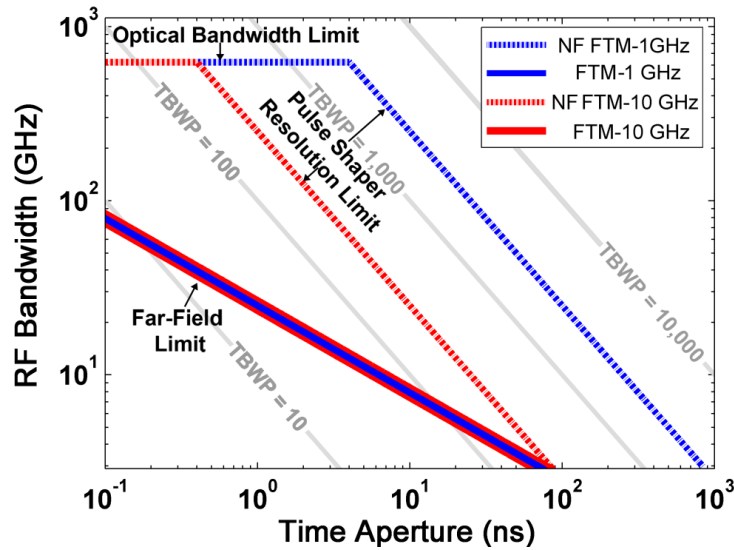


Fig. 7. Upper bounds of the achievable waveforms based on conventional FTM and NF-FTM for two shapers with assumed spectral resolutions of 1 GHz and 10 GHz and optical bandwidth of 5 THz. Conventional FTM is restricted to the space below the “far-field limit” for which good waveform fidelity is maintained, whereas NF-FTM is bounded only by the “optical bandwidth” and “pulse shaper resolution” limits.

is required for higher RF bandwidths, which reduces the maximum possible TBWP. The impact of our approach is especially clear for shapers operating at high spectral resolutions. For example, for a shaper with assumed 1 GHz resolution, a time aperture of 125 ns should be possible for frequencies up to 20 GHz (TBWP of $\sim 2,500$), while the time aperture would be limited to 1.56 ns (TBWP < 31) for the conventional technique (see section 4).

7. Conclusion

Frequency-to-time mapping is subject to the far-field condition, which imposes an onerous limit on the amount of information that can be placed on to the signal, severely restricting the time bandwidth product. We have introduced a new RF photonic AWG method which removes previous restrictions and achieves high fidelity waveforms with radically increased TBWP by predistorting the amplitude and phase of the spectrally shaped optical signal. The unprecedented instantaneous RF bandwidth of the generated waveforms offer potentials for new horizons in areas such as chirped radar, high-speed covert wireless, and RF sensing. Furthermore, by making use of state-of-the-art high speed photodetectors, our near-field frequency-to-time mapping technique can be applied for generation of arbitrary waveforms with RF frequency content well beyond that already demonstrated.

Appendix

Simulations and experiments presented in Figs. 3 and 5, respectively, showed that output intensity profiles obtained after dispersive propagation under conventional FTM were equal to scaled versions of optical power spectra shaped as prescribed under NF-FTM. Here we show that this scaling relationship always applies when $A_{FTM}(\omega)$, the Fourier transform of $a_{FTM}(t)$, is real.

We start with the power spectrum of the NF-FTM technique:

$$|A_{NF-FTM}(\omega)|^2 \propto \left| \int_{-\infty}^{+\infty} a_{NF-FTM}(t') \exp(-j\omega t') dt' \right|^2 \quad (16)$$

$$\stackrel{\text{equation (7)}}{=} \left| \int_{-\infty}^{+\infty} a_{FTM}(t') \exp\left(j \frac{t'^2}{2\psi_2}\right) \exp(-j\omega t') dt' \right|^2 \quad (17)$$

$$= \left| \left[\int_{-\infty}^{+\infty} a_{FTM}(t') \exp\left(j \frac{t'^2}{2\psi_2}\right) \exp(-j\omega t') dt' \right]^* \right|^2 \quad (18)$$

$$\stackrel{t' \rightarrow -t'}{=} \left| \int_{-\infty}^{+\infty} a_{FTM}^*(-t') \exp\left(-j \frac{t'^2}{2\psi_2}\right) \exp(-j\omega t') dt' \right|^2 \quad (19)$$

$$\stackrel{a_{FTM}^*(-t')=a_{FTM}(t')}{=} \left| \int_{-\infty}^{+\infty} a_{FTM}(t') \exp\left(-j \frac{t'^2}{2\psi_2}\right) \exp(-j\omega t') dt' \right|^2. \quad (20)$$

where the relation $a_{FTM}^*(-t) = a_{FTM}(t)$ holds based on the assumption that $a_{FTM}(t)$ has a real Fourier transform.

On the other hand, according to Eq. (1), the output intensity profile of the conventional FTM technique after dispersive propagation can be expressed as:

$$|a_{out}(t)|^2 \propto \left| \int_{-\infty}^{+\infty} a_{FTM}(t') \exp\left(-j \frac{t'^2}{2\psi_2}\right) \exp\left(j \frac{tt'}{\psi_2}\right) dt' \right|^2. \quad (21)$$

Equations (20) and (21) are scaled replicas of each other if we make the identification $\omega = -t/\psi_2$.

Acknowledgments

The authors would like to thank Dr. V. Torres-Company for his insightful comments, A. J. Metcalf for helping with figures, and Senior Research Scientist Dr. D. E. Leaird for his helpful technical assistance. This project was supported in part by the Naval Postgraduate School under grant N00244-09-1-0068 under the National Security Science and Engineering Faculty Fellowship program. Any opinion, findings, and conclusions or recommendations expressed in this publication are those of the authors and do not necessarily reflect the views of the sponsors.